Carrier-Wave Rabi Flopping and the Breakdown of the Area Theorem in Non-Linear Optics

Andrew Hayman[1, *]

[1] *Department of Physics, Engineering Physics and Astronomy, Queen's University, Kingston, ON K7L 3N6, Canada*

(Dated: January 28, 2022)

Two-level quantum systems exhibit carrier-wave Rabi flopping for ultra-high intensity driving fields. This results in the breakdown of the area theorem which can no longer predict the number of Rabi cycles. We demonstrate carrier-wave Rabi flopping and the breakdown of the area theorem with the optical Bloch equations using numerical methods. Low-intensity driving fields with and without the rotating wave approximation recover standard Rabi cycles, as predicted by the area theorem. For higher-intensity driving fields, carrier-wave Rabi flopping is observed. The power spectrum is computed for carrier-wave Rabi flopping and shows the presence of additional spectra, making power spectrum analysis a suitable method for verifying carrier-wave Rabi flopping experimentally.

I. INTRODUCTION

Two-level quantum systems are seen in a variety of fields such as non-linear optics, quantum computing and condensed matter physics. Driving the two-level system with a constant field causes the system to cycle between the two states, a phenomenon called Rabi flopping. By controlling and understanding Rabi flopping, we are enabled to accomplish a variety of applications such as quantum gate calibration in quantum computing and graphene-based device design [1][2].

The dynamics of a two-level quantum system can be simplified by making a rotating wave approximation (RWA). The RWA ignores the fast-rotating terms of the interaction Hamiltonian, placing the driving field in the frame of the two-level system. The number of Rabi cycles that occur for some driving field in the RWA can be found from the area theorem. Hughes has shown computationally that for large driving field areas, the area theorem breaks down due to carrier-wave Rabi flopping [3]. Mucke *et al.* has verified carrier-wave Rabi flopping experimentally with high intensity pulses in GaAs, and Ciappina *et al.* has shown computationally that it occurs in alkali species such as potassium atoms [4][5].

Here, we replicate the results of carrier-wave Rabi flopping and demonstrate the breakdown of the area theorem by solving the optical Bloch equations (OBEs) using numerical methods. First, we compare Euler's method and the 4^{th} order Runge-Kutta method (RK4) for ODE solving by comparing them to an analytical solution to the OBEs. Then, we simulate a Gaussian pulse in the RWA and examine the effects of dephasing and detuning. Finally, we examine carrier-wave Rabi flopping through Gaussian pulses without the RWA for a variety of pulse areas and frequencies, and the power spectrum is presented as a way of detecting carrier-wave Rabi flopping experimentally.

* 18arth@queensu.ca

II. THEORY AND EQUATIONS

Real two-level quantum systems can be described with a density matrix to account for non-pure states caused by effects such as polarization dephasing from system-bath interactions (Eq. 1). In this matrix, n_e is the population of the excited state, n_g is the population of the ground state where n_g=1-n_e, and $\rho_{eg} = \rho^*_{ge} = u$ is the coherence. When the coherence goes to zero, the non-diagonal elements go to zero, and we recover a pure quantum state.

$$\rho = \begin{pmatrix} n_e & \rho_{ge} \\ \rho_{eg} & n_g \end{pmatrix} \tag{1}$$

The OBEs describe two-level quantum systems interacting with an electromagnetic driving field, such as a laser pulse and have a different form depending on whether the RWA is used. They consist of a set of 1^{st} order coupled non-linear ordinary differential equations (ODEs) describing the complex coherence of the system and the population density of the excited state.

In the RWA, γ_d is the dephasing, $\Delta_{0L} = \omega_0 - \omega_L$ is the detuning where ω_L is the driving frequency and ω_0 is the frequency of the excited state, and $\tilde{\Omega}(t)$ is the time-dependent driving pulse:

$$\frac{du}{dt} = \gamma_d u - i\Delta_{0L} u + i\frac{\tilde{\Omega}(t)}{2}(2n_e - 1) \tag{2}$$

$$\frac{dn_e}{dt} = -\tilde{\Omega}(t)\mathrm{Im}[u] \tag{3}$$

The two driving fields used in this paper for the RWA are the continuous waveform and the Gaussian pulse where t_p is the time normalization:

$$\tilde{\Omega}(t) = \Omega_0 \tag{4}$$

$$\tilde{\Omega}(t) = \Omega_0 e^{(-t^2/t_p^2)} \tag{5}$$

Without the RWA, the fast oscillating parts are no longer ignored, leading to slightly different OBEs. The driving field changes from $\tilde{\Omega}(t)$ to $\Omega(t)$ to emphasize that it now must contain a carrier waveform at some frequency w_L,

and it follows that the detuning changes from Δ_{0L} to ω_0:

$$\frac{du}{dt} = -\gamma_d u - i\omega_0 u + i\Omega(t)(2n_e - 1) \tag{6}$$

$$\frac{dn_e}{dt} = -2\Omega(t)\mathrm{Im}[u] \tag{7}$$

The driving field used in this paper without the RWA is the Gaussian pulse with a carrier frequency given by:

$$\Omega(t) = \Omega_0 e^{(-t^2/t_p^2)} sin(\omega_L t + \phi) \tag{8}$$

Analytical solutions to the OBEs are available only for basic driving fields in the RWA, so numerical methods are required. The OBEs are 1st order coupled non-linear ODEs. Two methods for solving these types of differential equations are Euler's method with an $O(h)^2$ error (Eq. 9) and the RK4 method with an $O(h)^4$ error (Eq. 10-14) where h is the step size between iterations. Both methods require specifying a set of initial conditions.

$$y_{n+1} = y_n + hf(t_n, y_n) \tag{9}$$

$$y_{n+1} = y_n + \frac{1}{6}h(k_1 + 2k_2 + 2k_3 + k_4) \tag{10}$$

$$k_1 = f(t_n, y_n) \tag{11}$$

$$k_2 = f(t_n + \frac{h}{2}, y_n + h\frac{k_1}{2}) \tag{12}$$

$$k_3 = f(t_n + \frac{h}{2}, y_n + h\frac{k_2}{2}) \tag{13}$$

$$k_4 = f(t_n + h, y_n + hk_3) \tag{14}$$

The initial conditions for the OBEs in this paper are $t = 0$, $u = 0$ and $n_e = 0$, which assumes that the system starts in a fully coherent ground state. The step size is chosen to be $h = 0.001$ to increase accuracy except for the ODE solver comparison where $t = 0.01$, and the time normalization is set to $t_p = 1$ for all Gaussian pulses.

III. RESULTS

A. ODE Solver Comparison

First, we demonstrate that RK4 is a superior ODE solving method compared to Euler's method in terms of accuracy. We apply the continuous waveform in the RWA with no detuning ($\Delta_{0L} = 0$) and no dephasing ($\gamma_d = 0$). This system has a well known analytical solution:

$$n_e = sin^2(\Omega_0(t)) \tag{15}$$

A full Rabi oscillation takes $t = 1$ for a pulse amplitude of $\Omega_0 = 2\pi$ based on the area thereom:

$$A_{pulse} = \int dt\tilde{\Omega}(t) = \Omega_0 t \tag{16}$$

We compared the outputs of Euler's method and the RK4 method to the analytical solution (Fig. 1 and Fig. 2), demonstrating that RK4 outperforms Euler's method in accuracy. As a result, we have selected RK4 as the ODE solver for the rest of the paper.

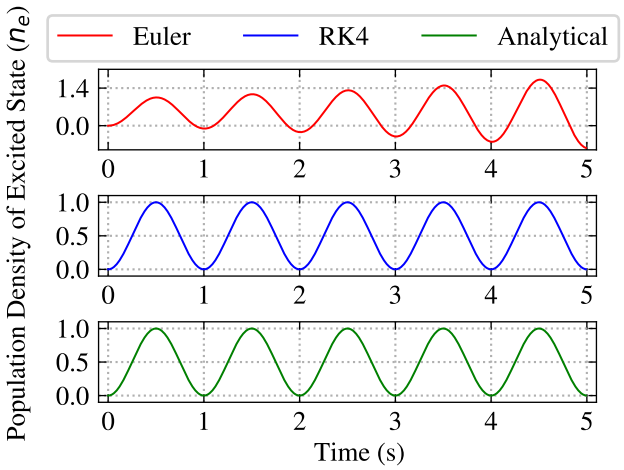

Figure 1. Population density of the excited state over time for a continuous 2π waveform in the RWA. Euler's method is observed to diverge rapidly.

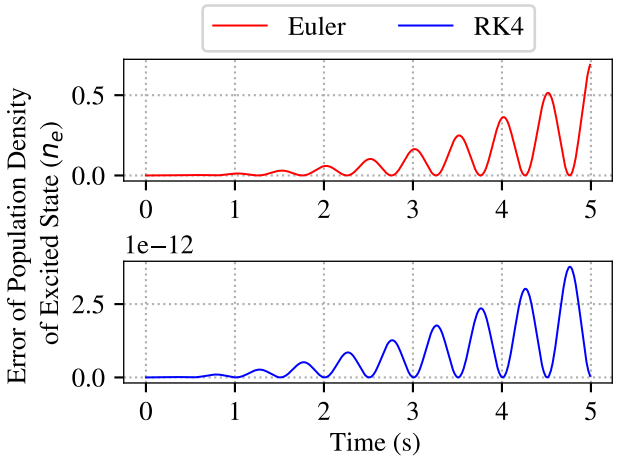

Figure 2. Squared error of population density of the excited state over time for a continuous 2π waveform in the RWA. While the qualitative shape of the methods are similar, the RK4 method shows a 10^{-12} magnitude better accuracy.

To benchmark our manually written RK4 against existing libraries, we compared run-times against SciPy's odeint solver in the integrate package. For no RWA where $t = 10$, $\Omega_0 = 2\sqrt{pi}$, $\omega_L = 4\sqrt{pi}$, and $\gamma_d = 0.4$, we found that SciPy was $\tilde{8}$ times faster than the manually written code. SciPy's odeint solver uses a different algorithm, called LSODA, making it challenging to directly compare performance.

B. Gaussian Waveform in the RWA

We then examined a Gaussian driving field in the RWA that achieves one full Rabi oscillation. One full Rabi oscillation requires a pulse area of 2π, and the required Ω_0

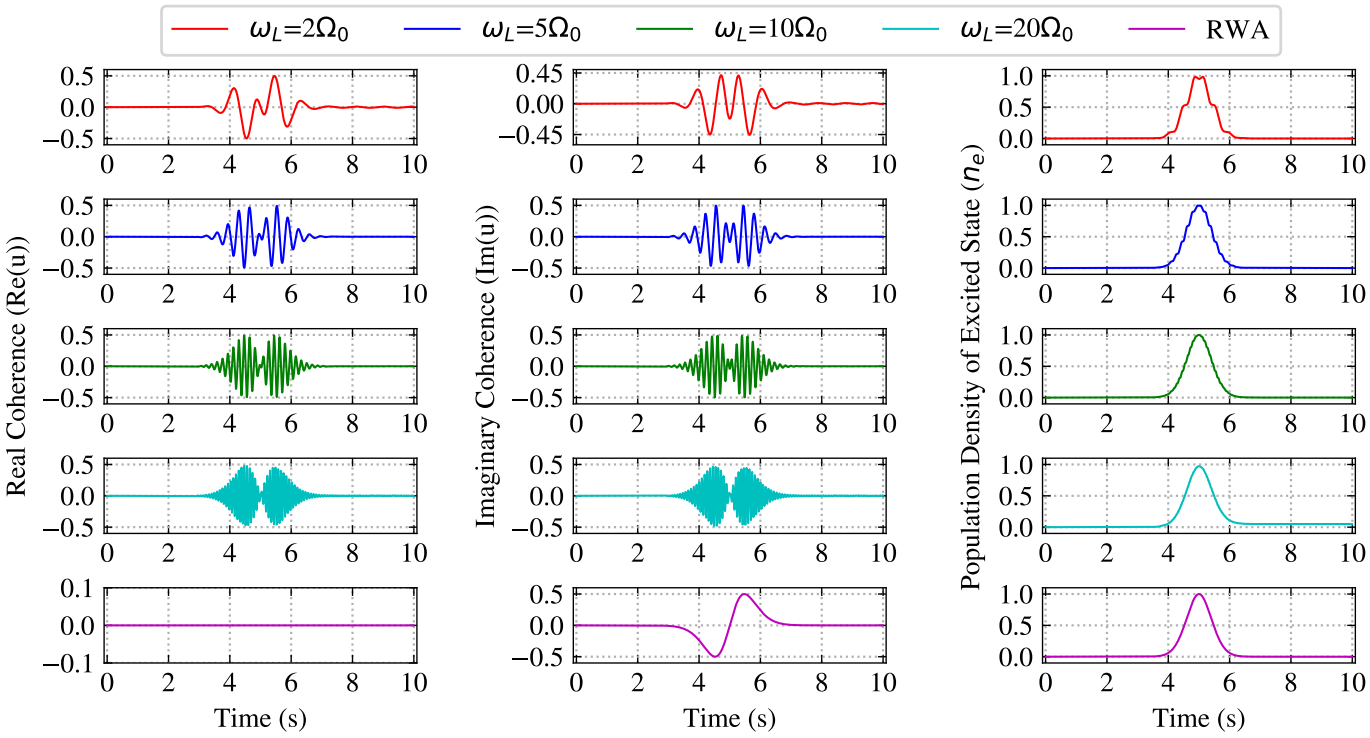

Figure 3. Population density of the excited state over time, illustrating a single Rabi flop from a driving Gaussian pulse with area 2π without the RWA. The slower the frequency, the more the effects of the carrier waveform are observed.

was calculated from the area theorem:

$$\begin{aligned} A_{pulse} &= \int dt\tilde{\Omega}(t) \\ 2\pi &= \int dt\Omega_0 e^{-(t/t_p)^2} \\ 2\pi &= \Omega_0\sqrt{\pi} \\ 2\sqrt{\pi} &= \Omega_0 \end{aligned} \tag{17}$$

The full effects of the Gaussian pulse are not observable if it is centered at $t = 0$ due to the initial condition of $t = 0$, so the pulse is given an offset of $t = 5$ for a final pulse equation of $\tilde{\Omega}(t) = 2\sqrt{\pi}e^{-(t-5)^2}$. No detuning ($\Delta_{0L} = 0$) or dephasing ($\gamma_d = 0$) were used initially. As expected, the system response shows a single Rabi oscillation (Fig. 4).

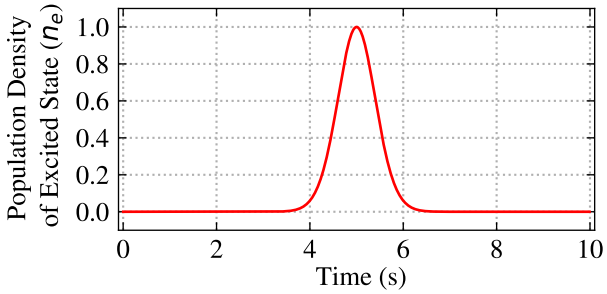

Figure 4. Population density of the excited state over time, illustrating a single Rabi flop from a driving Gaussian pulse with area 2π.

To investigate the effects of detuning and dephasing, we applied the same Gaussian pulse while varying the detuning and dephasing to see how the peak population of the excited state changes. The detuning, Δ_{0L}, was varied from 0 to Ω_0 with no dephasing ($\gamma_d = 0$) and the dephasing, γ_d, was simiarly varied from 0 to Ω_0 with no detuning ($\Delta_{0L} = 0$) (Fig. 5). As expected, a lower peak population is observed for both dephasing and detuning as they increase. We can also observe that dephasing effects cause a faster decrease in peak population than detuning.

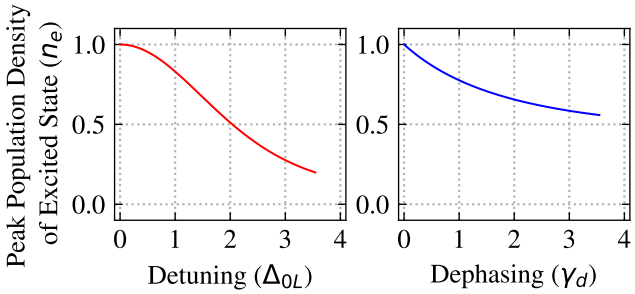

Figure 5. Peak population density of the excited state against dephasing and detuning, showing how dephasing and detuning decrease the effects of a driving pulse.

C. Gaussian Waveform without the RWA

Finally, we examine the same Gaussian driving field without the RWA to investigate carrier-wave Rabi flopping and the breakdown of the area theorem. The Gaussian pulse is modified to include the carrier waveform, $sin(\omega_L t + \phi)$, with $\Omega(t) = \Omega_0 e^{(-t^2/t_p^2)} sin(\omega_L t + \phi)$. We assume the driving field is on resonance with the system

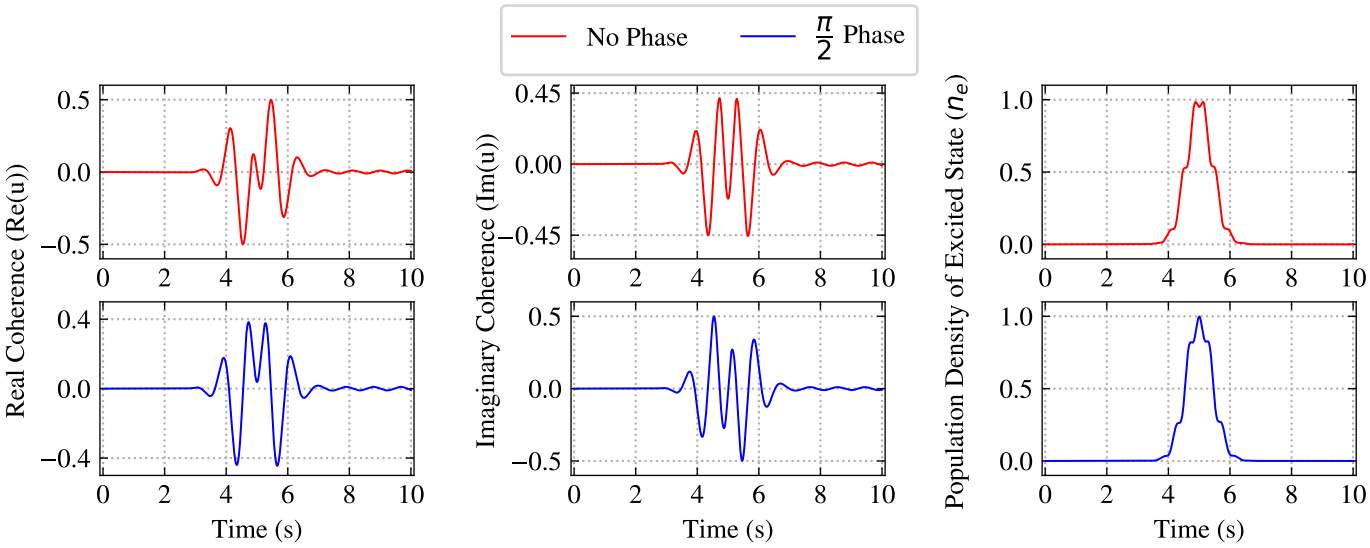

Figure 6. The coherence and population density are plotted with no phase and a phase of $\pi/2$ to demonstrate the effect of a phase shift in the carrier waveform. The single Rabi cycle is recovered, but a different qualitative form is observed.

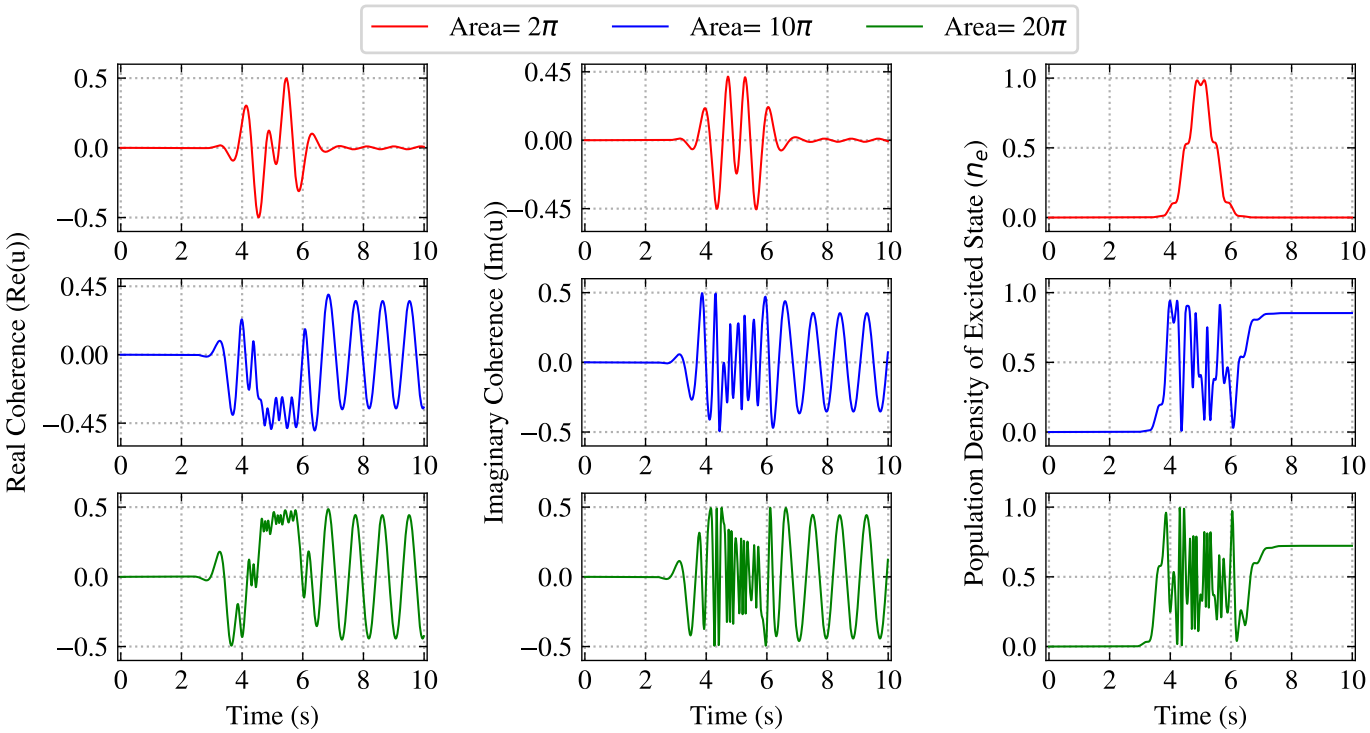

Figure 7. Coherence and population density from applying a set of pulse areas without the RWA. As the area increases, the area theorem no longer predicts the number of Rabi cycles. The 10π and 20π areas only complete 4.5 and 9.5 Rabi cycles instead of the 5 and 10 predict by the area theorem.

such that $\omega_0 = \omega_L$. First, we simulate a 2π pulse at a range of frequencies to illustrate how the RWA is a good approximation at high frequencies. We vary the phase of this pulse to examine the effects of a phase shift in the carrier waveform. Then, we fix the frequency, and increase the area of the system to show carrier-wave Rabi flopping. Finally, we take a Fourier transformation of the real coherence to see the power spectrum.

The frequency, ω_L, of the system and waveform is varied for a 2π pulse of $\Omega_0 = 2\sqrt{\pi}$ with no dephasing ($\gamma_d = 0$) at values of $\omega_L = 2\Omega_0$, $5\Omega_0$, $10\Omega_0$ and $20\Omega_0$. As expected, a single Rabi oscillation is recovered in all cases, validating the area theorem at low pulse intensities (Fig. 3). We can also observe that the RWA solution is approached as the frequency increases, because the RWA assumes the frequency is rapidly varying.

The phase is then changed from 0 to $\pi/2$ for $\omega_L = 2\Omega_0$ for the same 2π pulse (Fig. 6). A single full Rabi pulse is recovered, but with a different qualitative form due to the phase change. The RWA approximation does not account

for these effects, because it would add a global phase to the system's Hamiltonian, which is ignored. It does not however, make a difference to the solution, as the single Rabi cycle is still recovered.

The frequency of the system is now fixed at $\omega_L = 4\sqrt{\pi}$ with no dephasing ($\gamma_d = 0$) and the pulse area is varied with values of 2π, 10π and 20π. Here, carrier-wave Rabi flopping is observed along with the breakdown of the area theorem (Fig. 7). The 2π area recovers a single Rabi cycle, as predicted from the area theorem. However, the 10π area shows 4.5 cycles instead of the expected 5 from the area theorem. Similarly, the 20π area shows 9.5 cycles instead of the expected 10 from the area theorem.

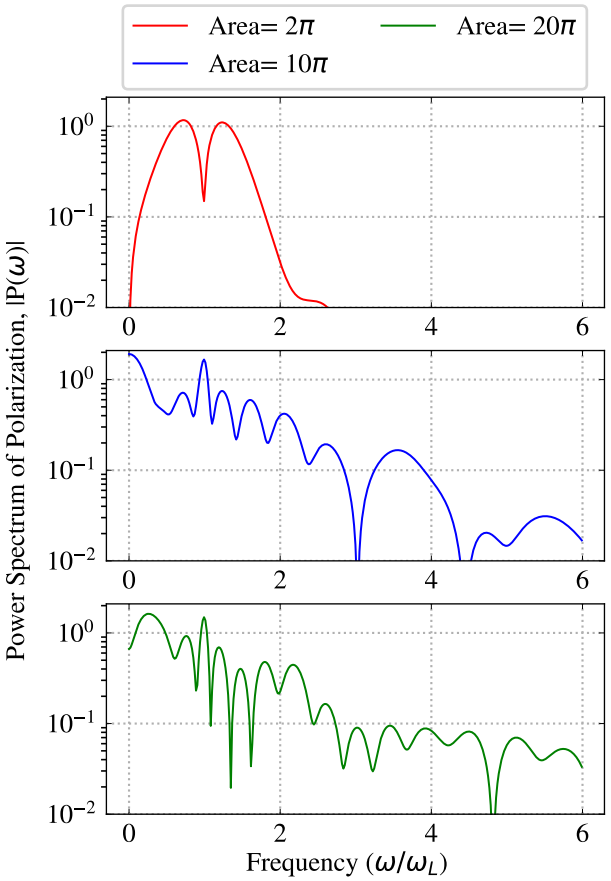

Figure 8. Power spectrum of polarization, showing a variety of lower and higher spectral components at higher intensities where the area theorem breaks down and carrier-wave Rabi flopping is observed.

We can verify carrier-wave Rabi flopping experimentally by checking for the presence of high-frequency components in the output power spectrum. Here, we examine the output power spectrum where the power spectrum is $P(\omega) \propto Re(u)$. Consider the same 2π, 10π and 20π pulses on resonance at $\omega_L = 2\Omega_0$, but with a polarization dephasing of $\gamma_d = 0.4$ and a time of $t = 50$. The 2π pulse shows a two-beat pattern with a spectral hole while the higher area pulses with carrier-wave Rabi flopping show the addition of both higher and lower frequencies (Fig. 8). As the frequency of the driving pulse is increased, the single power spectrum value of w_L is recovered. By measuring the spectrum of the output pulse, the presence of carrier-wave Rabi flopping can be observed, as suggested by Hughes [3].

IV. CONCLUSION

We have demonstrated the effects of carrier-wave Rabi flopping computationally, as well as a method for measuring it experimentally. The optical Bloch equations with and without the RWA were solved with the RK4 method for a variety of conditions. A Gaussian pulse in the RWA was used for a single Rabi flop to demonstrate the area theorem. Including the dephasing and detuning of the experiment led to a decrease in peak population of the expected state, as expected. A 2π pulse without the RWA was shown at a variety of frequencies to show how larger frequencies approach the results from the RWA. The effects of the phase in the carrier waveform were investigated with no effect on the Rabi flopping. Large pulse areas were investigated, and showed the effects of carrier-wave Rabi flopping and the breakdown of the area theorem. Finally, the input and output power spectra were compared for cases with and without carrier-wave Rabi flopping to demonstrate that the effects can be verified experimentally by checking for frequencies lower and higher than the driving frequency.

Future computational work could be done on the timescales and length-scales of real physical systems which can be verified experimentally, as demonstrated by Hughes, and Ciappina *et al.* [3][5].

References

[1] Li Yang, Biyao Yang, and Yufu Chen, "Full quantum treatment of rabi oscillation driven by a pulse train and its application in ion-trap quantum computation," (2013), arXiv:1010.5986 [quant-ph].

[2] Feng Wang, Chengzhi Qin, Bing Wang, Hua Long, Kai Wang, and Peixiang Lu, "Rabi oscillations of plasmonic supermodes in graphene multilayer arrays," IEEE Journal of Selected Topics in Quantum Electronics **23**, 125–129 (2017).

[3] S. Hughes, "Breakdown of the area theorem: Carrier-wave rabi flopping of femtosecond optical pulses," Phys. Rev. Lett. **81**, 3363–3366 (1998).

[4] O. D. Mücke, T. Tritschler, M. Wegener, U. Morgner, and F. X. Kärtner, "Signatures of carrier-wave rabi flopping in gaas," Phys. Rev. Lett. **87**, 057401 (2001).

[5] M. F. Ciappina, J. A. Pérez-Hernández, A. S. Landsman, T. Zimmermann, M. Lewenstein, L. Roso, and F. Krausz, "Carrier-wave rabi-flopping signatures in high-order harmonic generation for alkali atoms," Phys. Rev. Lett. **114**, 143902 (2015).